Investigation of the Benefits of Combined GPS/GLONASS for High Sensitivity Receivers

C. O'Driscoll, M.E. Tamazin, D. Borio and G. Lachapelle
Position, Location and Navigation Group
Department of Geomatics Engineering
Schulich School of Engineering
University of Calgary

BIOGRAPHY

Dr. Cillian O'Driscoll received his Ph.D. in 2007 from the Department of Electrical and Electronic Engineering, University College Cork. His research interests are in the area of software receivers for GNSS, particularly in relation to weak signal acquisition and ultra-tight GPS/INS integration. He is currently with the Position, Location and Navigation (PLAN) group at the Department of Geomatics Engineering in the University of Calgary.

Mohamed Tamazin is a M.Sc. candidate in the Position, Location And Navigation (PLAN) group at the Geomatics Engineering Department in the University of Calgary. He also holds a B.Sc. and M.Sc. in Electrical Communications from Arab Academy for Science and Technology (AAST), Alexandria, Egypt. His current research focuses on the field of wireless communication, location and integrated navigation systems.

Daniele Borio received the M.S. degree in Communication Engineering from Politecnico di Torino, Italy, the M.S. degree in Electronics Engineering from ENSERG/INPG de Grenoble, France, in 2004, and the doctoral degree in electrical engineering from Politecnico di Torino in April 2008. He has been a senior research associate at the PLAN group of the University of Calgary, Canada, since January 2008. His research interests include the fields of digital and wireless communication, location, and navigation.

Prof. Gérard Lachapelle is a Professor of Geomatics Engineering at the University of Calgary where he is responsible for teaching and research related to location, positioning, and navigation. He has been involved with GPS developments and applications since 1980. He has held a Canada Research Chair/iCORE Chair in wireless location since 2001 and heads the PLAN Group at the University of Calgary.

ABSTRACT

High Sensitivity (HS) GNSS receivers have flourished in the last decade. A variety of advances in signal processing techniques and technologies have led to a thousandfold decrease in the minimum useable signal power, permitting use of GNSS, in particular GPS, in numerous environments where it was previously impossible.

Despite these recent advances, the issue of availability remains: in many scenarios there are simply too few satellites available with detectable signals to compute a position solution. Of course one way to improve this situation is to increase satellites availability. It is well known that GLONASS has been undergoing an accelerated revitalization program of late, such that there are currently 20 active GLONASS satellites on orbit. The combined use of GPS and GLONASS in a high sensitivity receiver is a logical one, providing a near two-thirds increase in the number of satellites available for use.

This paper investigates the benefits of adding GLONASS capability to the GSNRx™ software receiver in high sensitivity (HS) mode. The analysis focuses on the issues of availability and accuracy, both of pseudorange measurements and navigation solutions. The impact of the system time offset is also taken into consideration. The analysis is based on the collection of synchronous data from an outdoor, reference antenna with a clear view of the sky, and an indoor rover antenna. Raw IF samples are captured and processed post-mission to observe with a very fine level of detail the signals deep indoors.

INTRODUCTION

High Sensitivity (HS) GPS receivers have flooded the world in the last decade. Driven primarily by the E-911 mandate from the FCC, these devices have become

almost ubiquitous on modern smart phones. However, there are still many scenarios in which the number of satellites observable with these devices is insufficient to compute a navigation solution. With the recent revitalization of the Russian Global Navigation Satellite System (GLONASS), with a constellation of 24 satellites by the end of 2010, it is worthwhile to concentrate on the GLONASS system as a method of GPS augmentation to achieve more reliable and accurate navigation solutions as was shown over a decade ago when GLONASS was also nearly complete (e.g. Lachapelle et al 1997).

The addition of GLONASS capability to a GPS receiver introduces a number of design challenges, not least of which is the requirement for extra RF bandwidth, either in the form of a second front-end stage, or in a dramatic increase in the bandwidth of the existing front-end. For the purposes of this paper, it will be assumed that the required RF bandwidth is available for processing, without consideration for the extra cost involved. A second issue that arises is the asynchronicity of GPS and GLONASS, which introduces an unknown, potentially time varying, bias between the time scales of the two systems (GLONASS ICD 2002). In this paper, two approaches are considered for dealing with this unknown bias. The first approach treats it as a parameter to be estimated, thereby requiring more signal observations to be made so as to obtain a navigation solution. The second approach is to assume that the bias is sufficiently stable that it can be provided to the high sensitivity receiver through a secondary data link, or can be estimated in clear sky conditions and stored for use in degraded signal environments.

The methodology used in this paper is based on a characterization of the received signal strength of both GPS and GLONASS L1C/A signals in a variety of indoor environments. Processing is conducted on raw Intermediate Frequency (IF) samples collected synchronously from antennas at two locations, one with a clear view of the sky (the reference), and one in a degraded environment (the rover). The front-ends used to collect this data are driven by the same local oscillator, thereby ensuring that both reference and rover data are subject to the same clock bias and drift effects. While this setup permits the observation of the signals at very low C/N_0, thereby determining precisely their behavior in these regimes, it is not a realistic approach for real-time navigation. The results obtained are, however, indicative of the best that can be achieved using HS-GNSS receivers, neglecting receiver oscillator errors.

Data has been collected in two test scenarios, namely in a suburban home and in an engineering laboratory. Analysis focuses on the accuracy of the measurements and the availability and accuracy of single point, epoch-by-epoch least-squares solutions. In this way the impact of a smoothing navigation filter does not mask the real errors.

Section 2 introduces the methodology adopted in this paper. The test setup and the obtained results are presented in Sections 3 and 4 and, finally, conclusions and future work are discussed in Section 5.

METHODOLOGY

Due to the extreme nature of the attenuation and fading experienced by GNSS signals indoors, analyzing their behavior poses some significant challenges. Three possible solutions can overcome these problems. Firstly, a high sensitivity (HS) standalone/assisted GPS/GLONASS receiver may be used (Watson et al 2005). Secondly, measurements from a pair of receivers, a reference and a rover, which are synchronized to a very high accuracy, may be used (Haddrell & Pratt 2001, Mitelman et al 2006, Satyanarayana et al 2009). Finally, GPS/GLONASS-like signals with a very high gain transmitter may be generated in order to overcome the high level of attenuation caused by the external walls and rooftops.

In this paper, the two-receiver configuration is used to process indoor GPS/GLONASS L1 C/A signals. In this method, measurements obtained from the reference receiver placed in outdoor conditions with a clear view of the sky, can be effectively used to compute Doppler frequency, code phase and data bits, which can be wiped off the indoor signals, thus enabling long coherent integration for the indoor receiver (the rover) placed in a degraded environment.

The data is processed with a modified version of the GNSS Software Navigation Receiver (GSNRx™), (O'Drisoll et al 2009). This reference/rover based version is called GSNRx-rr™, which is a C++ class-based GNSS receiver software program capable of processing data samples from one reference and several rover front-ends in post-mission (Satyanarayana et al 2009). All signals in view at the reference antenna are acquired and tracked in a phase locked mode. This data is then used to wipe-off the code, carrier and data bits from the signals collected from the rover antenna. A grid of correlator points are computed at a variety of code phase and Doppler offsets around the reference values. This configuration is illustrated schematically in Figure 1.

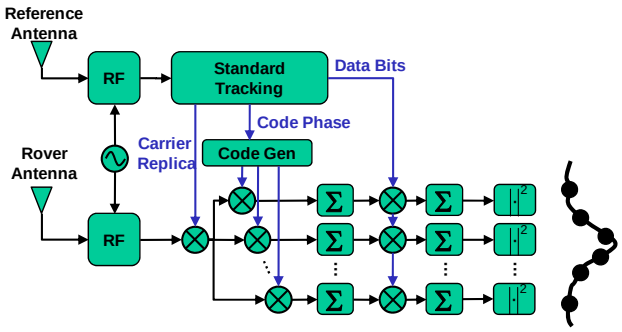

Figure 1: Schematic of GSNRx-rr™.

The use of the reference values for data, code and carrier means that the rover data can be correlated over very long coherent integration times, permitting the computation of the cross ambiguity function of the rover data even for very weak signals. Using this grid of correlator values, various signal parameters including C/N_0, delta pseudorange and delta frequency can be computed. In this work, the focus is on pseudorange measurements in a static environment, so the Doppler measurements from the reference receiver are used directly. The correlator grid has been chosen to span +/- 2 chips around the reference code phase in 0.1 chip increments. In this way a very fine level of detail can be observed, in addition to long range multipath (greater than 1 chip delay), should it exist.

For the purpose of this work, a coherent integration time of one second was chosen. This permits the reliable observation of signals with C/N_0 as low as 10 dB-Hz. In addition, the long integration helps reduce the impact of cross-correlation and other RF interference. As such, the measurements generated in this configuration represent a best case. These parameters are not easily achievable in practice without the aiding provided by the reference antenna.

Once the grid of correlators has been computed, a simple quadratic interpolation is used to determine the location of the peak code phase. In the case that there is no multipath, this represents a reasonable approximation to the maximum likelihood estimate of the code phase difference between the reference and the rover. Pseudorange difference measurements can then be made directly by scaling the code phase to units of length. The error model adopted for this delta pseudorange measurement is given by

$$\Delta PR = \Delta R + \Delta MP + \Delta n + c\Delta t_p \qquad \textbf{(1)}$$

where ΔPR is the delta pseudorange measurement, ΔR is the true range difference, ΔMP is the difference between the multipath error in the reference measurement and that in the rover measurement, Δn is the difference in the thermal noise contributions of the two measurements, c is the speed of light and Δt_p is the differential delay due differences in cable lengths connecting the reference and rover antennas to their respective front-ends.

The final stage in the methodology is the computation of position solutions at the rover. To this end the measurements are post-processed to generate a position and clock only (no velocity) solution using a weighted least-squares algorithm with blunder detection and removal. The measurements are weighted using a standard elevation dependent model, which has not been tuned for the particular scenarios tested. The position solutions are computed using three separate approaches:

1. Using GPS measurements only (denoted GPS)
2. Using both GPS and GLONASS measurements, and estimating the GPS/GLONASS system time offset (denoted GLO)
3. Using both GPS and GLONASS measurements, and providing the system time offset estimated from the reference measurements (denoted GG+CLK).

The results are compared in terms of solution availability, accuracy and geometry (PDOP).

TEST SETUP & DESCRIPTION

Data were collected using five National Instruments PXI-5661 front-ends, in two separate chassis, and two NovAtel GPS702-GG model antennas. The NovAtel GPS702-GG antenna can receive GPS and GLONASS L1 and L2 signals. The first antenna was placed on the rooftop with a clear view of the sky and used as a reference, while the second one was placed in a degraded environment (the rover). Figure 2 shows the test setup adopted for collecting synchronous live GPS/GLONASS L1 C/A signals. The reference signal was passed through a low noise amplifier followed by splitter where it was divided into three signals. One of these signals was passed to the first NI chassis, where it serves as the source of reference GPS data. The other two were passed to the second NI chassis, one of which serves as a source of the GLONASS reference data, the second of which is used to provide precise sample level synchronization between the two chassis.

The front-ends used to collect this data are driven by the same local oscillator, thereby ensuring that both reference and rover data are subject to the same clock bias and drift effects. In the font-ends, the signals were sampled and down converted into desired intermediate frequency.

In the case of the rover antenna, the same setup was used, minus the extra synchronization signal. Digitized samples from the NI system were stored on an external hard drive and later processed with GSNRx-rr™.

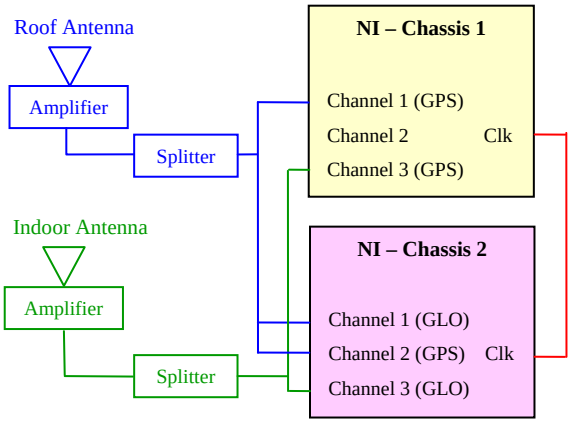

Figure 2: Test setup adopted for collecting synchronous live GPS/GLONASS L1 C/A signals.

Data was collected in two test scenarios, namely in a typical North American Wooden House (WH) and in an engineering laboratory (NavLab) inside the Calgary Center for Innovative Technologies (CCIT) building of the University of Calgary. The specifications of the digitized signals are reported in Table 1.

Table 1: Settings adopted for the data collection.

Parameters	GPS Signal	GLONASS Signal
Sampling Frequency (MHz)	5 (WH) 12.5 (NavLab)	12.5
IF Frequency (MHz)	0.42	0
Sampling	Complex	Complex
Quantization Bits	16	16

EXPERIMENTAL RESULTS & ANALYSIS

In this section, the results obtained using GSNRx™ for the two experiments described above are detailed. The section includes results from the combined GPS and GLONASS systems in terms of detection, measurement and position accuracy.

Wooden House Results

This type of wooden house represents a relatively benign indoor environment, but still poses significant challenges to standard receivers. Signal attenuation was of the order of 5 to 25 dB, with most signals attenuated by less than 15 dB. The locations of the reference and rover antennas are illustrated in Figure 3 and Figure 4 respectively. The test lasted just under 10 minutes, with a 1 Hz solution rate a total of 564 solutions were possible.

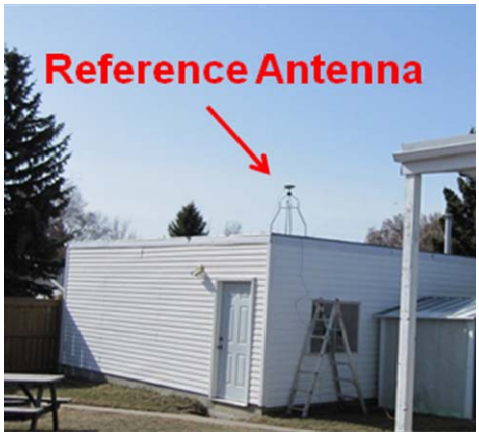

Figure 3: Location of reference antenna for the WH test

Figure 4: Location of rover antenna for the WH test

The skyplot of the satellites visible at the start of the test is shown in Figure 5. As can be seen, there were 11 GPS and 6 GLONASS satellites in view. The test duration was approximately 10 minutes and there was little variation in geometry for the duration of the test.

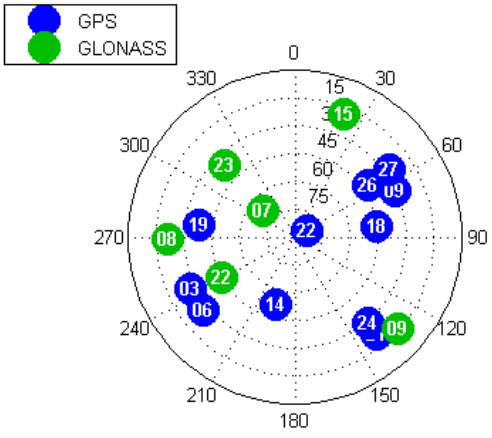

Figure 5: Skyplot for the start of the WH test

Some sample correlator outputs are shown in Figure 6 and Figure 7. The impact of fading is clearly visible in each of these plots, while the effect of the instantaneous multipath is not readily discerned: a visual inspection shows one clear peak in each epoch, indicating that the multipath is all close range. This is to be expected given that most of the significant reflectors are within a few metres or tens of metres of the rover antenna.

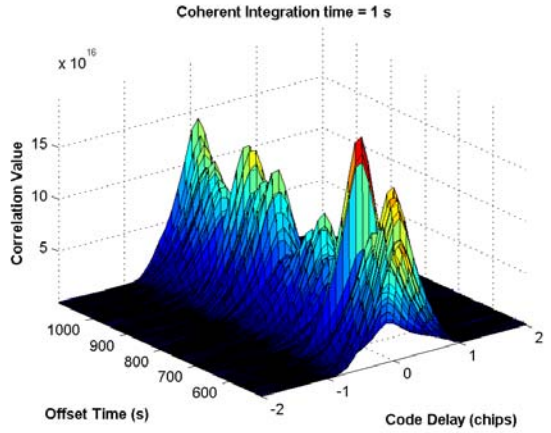

Figure 6: Time series of correlator outputs for GPS PRN 6: 1 second coherent integration time

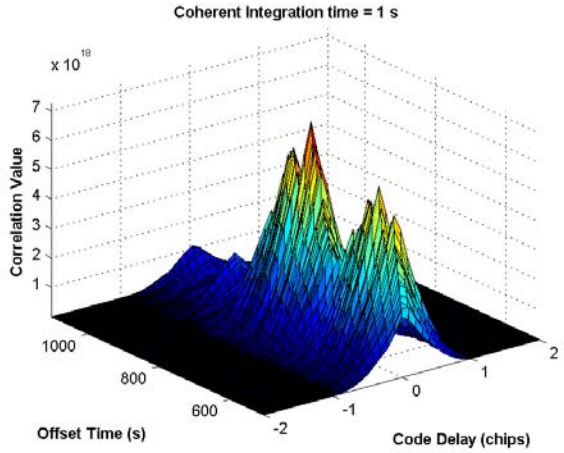

Figure 7: Time series of correlator outputs for GLONASS PRN 9: 1 second coherent integration time

The C/N_0 estimated from the rover correlator outputs is illustrated in Figure 8 and Figure 9 for GPS and GLONASS satellites, respectively.

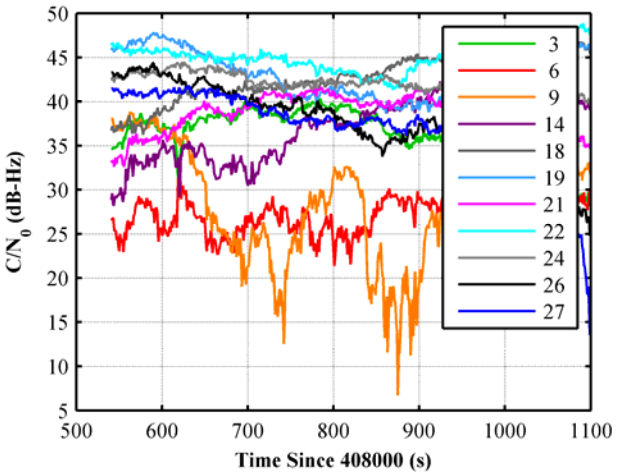

Figure 8: Carrier-to-noise density ratio of the GPS signal received on the main floor of the WH.

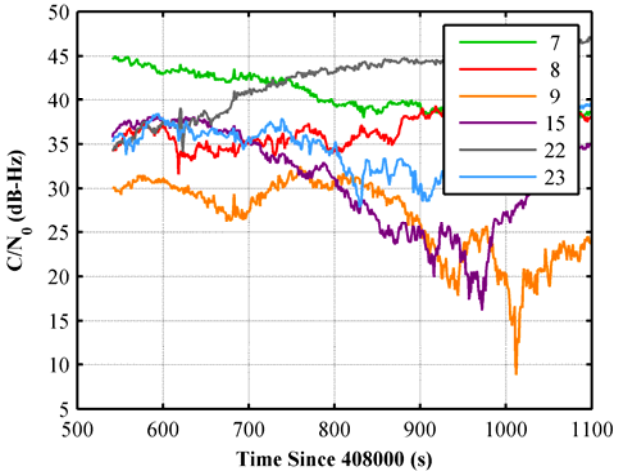

Figure 9: Carrier-to-noise density ratio of the GLONASS signal received on the main floor of the WH.

As might be expected, both the levels and the trends observed in the C/N_0 values are very similar between GPS and GLONASS. While the two signals are in slightly different frequency bands, the fading environment appears very similar in each case. This is encouraging, as it suggests that high sensitivity processing that has been developed for GPS will be equally effective for GLONASS.

The next logical step is to compare the pseudorange measurement quality. Unfortunately for this test the true position of the rover antenna is not available. Thus, it is not possible to directly observe the RMS errors. Figure 10 shows the estimated standard deviations of the GPS and GLONASS delta pseudorange measurements as a function of C/N_0. GLONASS measurements should be noisier than those of GPS, due to the longer chip length in GLONASS.

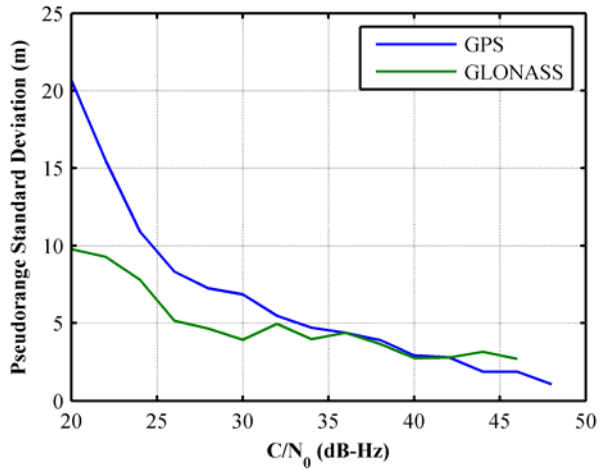

Figure 10: Delta pseudorange standard deviations vs C/N_0 for the WH test

Figure 10 was obtained by dividing the measurements into bins based on the estimated C/N_0 values. The trend of increasing standard deviation with decreasing C/N_0 is to be expected. However, it would also be expected that the GLONASS measurements should be noisier than the GPS measurements, due to the lower chipping rate of the GLONASS C/A code. As can be seen from the figure, the opposite appears to hold in this case. Though, it must be acknowledged that the number of observations at the lower end of the C/N_0 scale is low, leading to a less accurate estimate of the pseudorange standard deviation. In reality, it appears that the measurement errors in this case are approximately the same for the two systems.

Referring to Eq. (1), it can be seen that the major contributors to the estimated standard deviations will be the rover thermal noise errors and the temporal variation of the rover multipath error. The true range difference ΔR varies by only a few decimetres at most and does not contribute to the standard deviations. The Δt_p term should be constant throughout the test.

A scatter plot of the horizontal positions computed is given in Figure 11. Recall that the three solutions correspond to: 1) GPS only measurements, 2) GPS plus GLONASS measurements, with estimation of the system time offset, 3) GPS plus GLONASS measurements with provision of the system time offset.

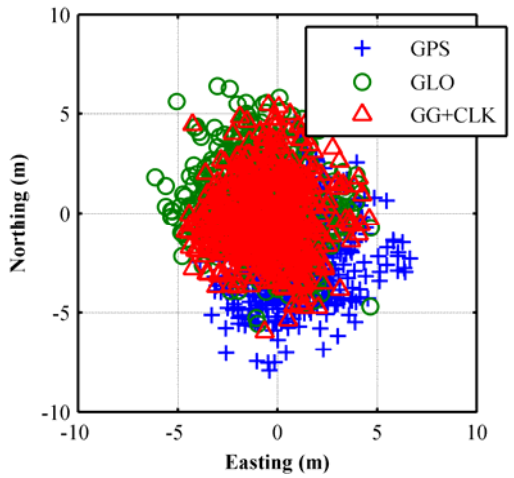

Figure 11: Scatter plot of horizontal positions computed for the WH test. The origin is given by the mean value of the GG+CLK case

The position results are broadly similar for all three cases (in the figure, the origin is obtained as the average position from the GG+CLK results).

Figure 12 shows the percentage of the time the least-squares algorithm was able to converge on a valid solution. Here the position solution was obtained by setting a minimum C/N_0 threshold. Measurements for which the C/N_0 was below the threshold were not considered by the navigation solution. Thus, the performance of receivers with different levels of sensitivity can be compared, with the caveat that the measurements generated here are less susceptible to interference than less sensitive receivers due to the 1 s integration time. For this environment, all three approaches yielded almost 100 % solution availability for all reasonable levels of receiver sensitivity.

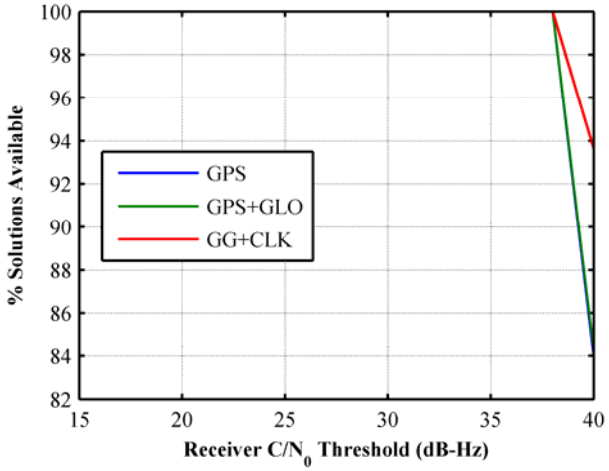

Figure 12: Percentage solution availability vs receiver sensitivity for the WH test. Note that 100 % availability is seen in most cases

The impact of adding GLONASS on geometry is evaluated by comparing the PDOP for each of the three cases. Figure 13 shows the mean, maximum and minimum PDOP values observed in each case. There appears to be an approximately 30 % improvement in PDOP when adding GLONASS in this case, but the values for GPS alone are already quite good, given the environment.

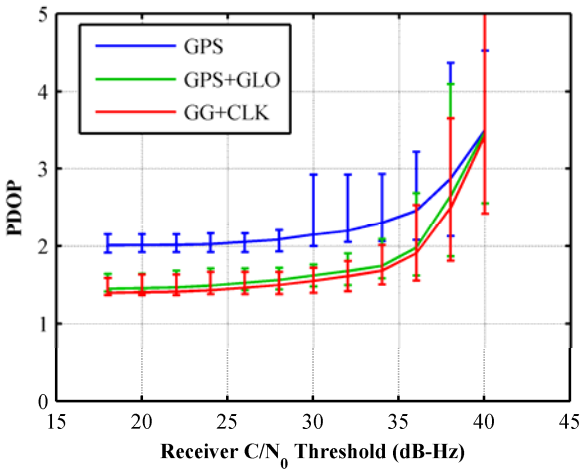

Figure 13: Mean, max and min PDOP vs receiver sensitivity for the WH test. The continuous lines represent the mean value, the error bars report the maximum and minimum

Figure 14 and Figure 15 show the standard deviations in the horizontal and vertical positions for each of the three processing cases as a function of receiver sensitivity. There is very little difference between the GPS only and the GPS plus GLONASS solutions in this case, with some improvement in the vertical positions when GLONASS is added.

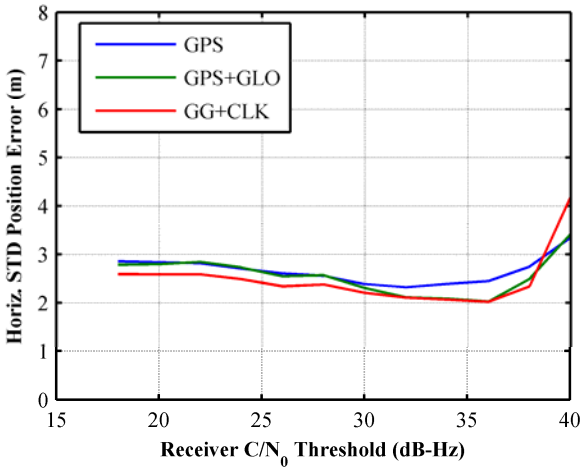

Figure 14: Standard deviation of the horizontal positions vs receiver sensitivity for the WH test

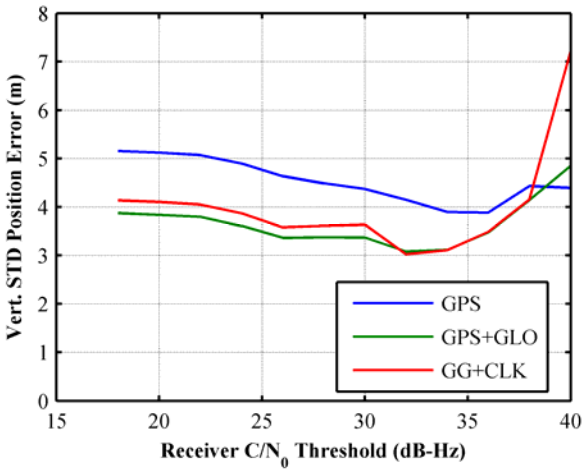

Figure 15: Standard deviation of the vertical positions vs receiver sensitivity for the WH test

The results of this test are encouraging, in that the GLONASS measurements are of similar quality to those of GPS, and some minor improvements in positioning performance were observed. However, the benefit of adding GLONASS in this type of environment appears to be minimal from an accuracy and availability point of view.

Engineering Laboratory Results

For this scenario the reference antenna was installed on the roof of the CCIT building while the rover antenna was placed in the Navigation Laboratory (NavLab) one floor below the roof. This represents an extremely challenging environment for GNSS signals, with multiple reflectors at close range and a high degree of attenuation in most directions, namely of the order of 15 to 45 dB. The lab also contains a significant amount of electronic equipment, two pieces of which were found to produce RF interference in the L1 band. For the purpose of this test these interferers were switched off. This test lasted just under 8 minutes and for a measurement rate of 1 Hz, just over 460 position solutions were generated.

The locations of the reference and rover antennas are shown in Figure 16. These locations are both known to within a few centimetres, which permits the computation of absolute range and position errors for the purposes of comparison in the following analysis.

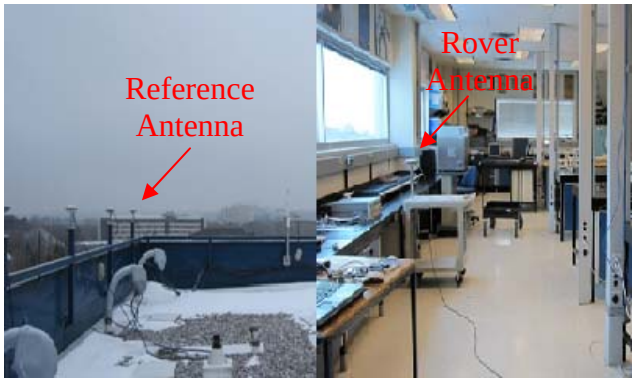

Figure 16: Locations of the reference and rover antennas for the NavLab test. Both pictures are taken looking south.

The sky plot at the start of the test is shown in Figure 17. In this case there were 11 GPS and 6 GLONASS satellites in view, with excellent coverage of the sky.

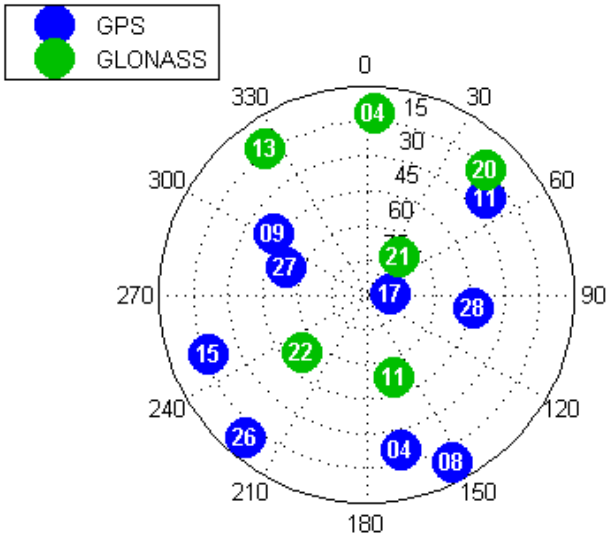

Figure 17: Skyplot at the start of the NavLab test

The time series of the correlator outputs for a GPS and a GLONASS satellite are shown in Figure 18 and Figure 19 respectively. As with the WH test, the effect of fading is clearly visible in these plots, and the fading appears to be due mostly to short range multipath. Similar plots were observed for all satellites in view.

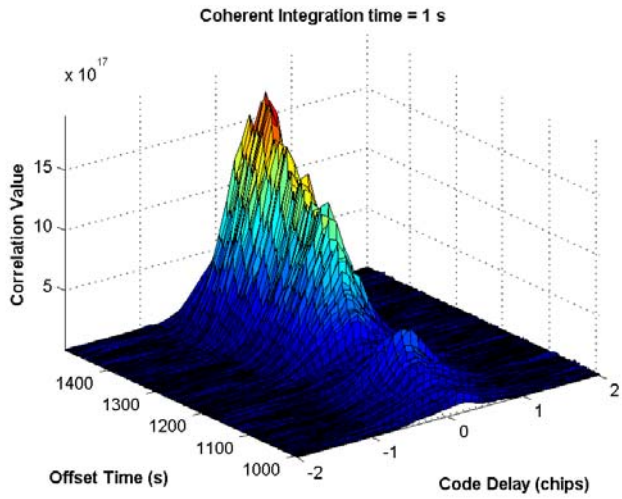

Figure 18: Time series of correlator outputs for GPS PRN 27: 1 second coherent integration time

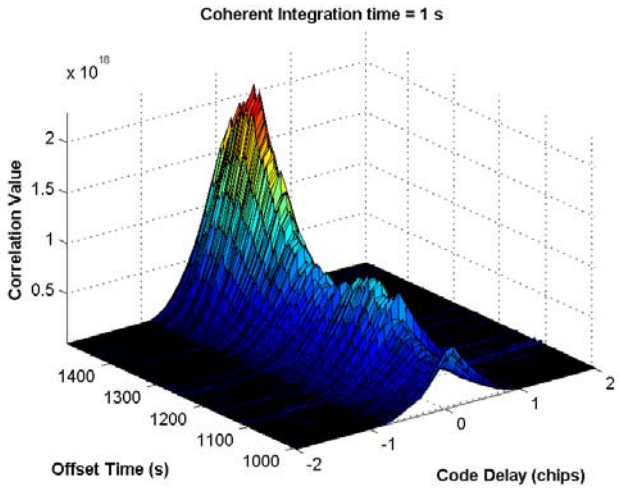

Figure 19: Time series of correlator outputs for GLONASS PRN 22: 1 second coherent integration time

Figure 20 and Figure 21 show the measured C/N_0 at the rover antenna for GPS and GLONASS satellites, respectively. Clearly this environment is considerably more challenging than that of the WH scenario: most signals are in the 5 to 15 dB-Hz range (though C/N_0 values below about 5 dB-Hz cannot be reliably estimated with a 1 s integration time). Interestingly, the signal from GLONASS PRN 22 was received with relatively high power. This satellite was at a reasonably high elevation to the south west and may have been reflected through one of the windows.

.

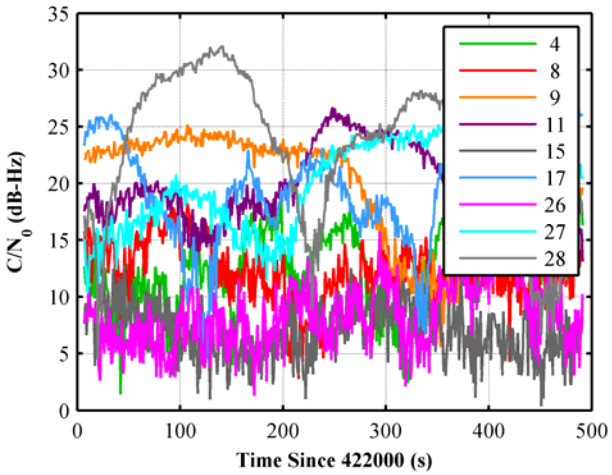

Figure 20: GPS C/N_0 vs time for the NavLab test

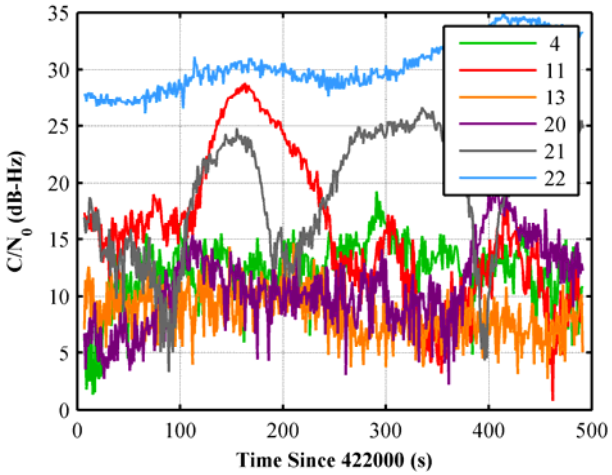

Figure 21: GLONASS C/N_0 vs time for the NavLab test

To compare the quality of the pseudorange measurements of GPS and GLONASS in this case, the known positions of the reference and rover antennas are used to compute the ΔR term of Eqn. (1). The remaining terms in this equation are the multipath and thermal noise terms (which are to be evaluated), and the differential propagation time Δt_p. Unfortunately this term was unknown due to the unknown propagation time of the signal from the roof mounted antenna. Instead this term was estimated by computing a fixed point navigation solution with the rover measurements. Thus the estimated differential propagation time also includes the average differential multipath errors.

A corrected pseudorange measurement was then computed for each satellite as

$$\Delta\rho = \Delta PR - \Delta R - c\widehat{\Delta t_p} \qquad \textbf{(2)}$$

The RMS values of these corrected pseudorange measurements as a function of C/N_0 are illustrated in Figure 22 (note that the RMS values are plotted on a log scale).

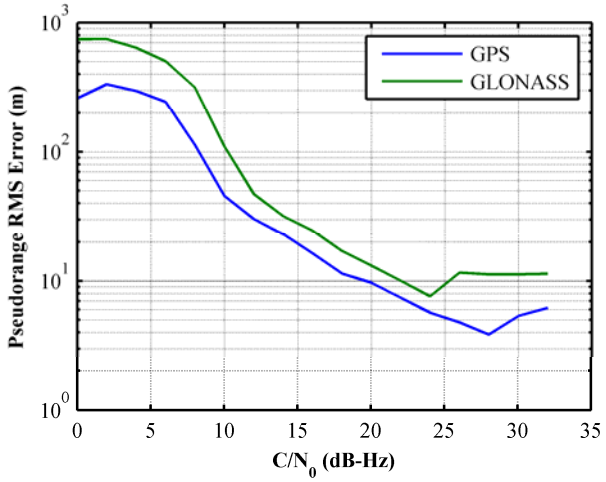

Figure 22: RMS pseudorange error vs receiver sensitivity for the NavLab test

A few interesting points can be noted from this plot. Firstly, in the mid C/N_0 range (10 – 22 dB-Hz), the curves are both linear and parallel, as would be expected. Secondly, the GLONASS measurements are noisier than the GPS measurements, in contrast to what was observed in the WH scenario, but in line with expectations. Finally, the estimated RMS values plateau at lower C/N_0 values, in this case the signal is buried in the noise and the distribution of the measurements tends to the uniform distribution.

Of critical importance, however, is the fact that the measurements of each system appear to be useable (of the order of 5 – 50 m RMS errors) for C/N_0 values greater than about 10 dB-Hz, for the 1 s coherent integration time case. A scatter plot of the horizontal position errors computed using the three processing strategies and a minimum C/N_0 threshold of 10 dB-Hz is shown in Figure 23. Note that all position solutions are computed using the raw (i.e. ΔPR rather than $\Delta\rho$) pseudorange measurements from the rover antenna.

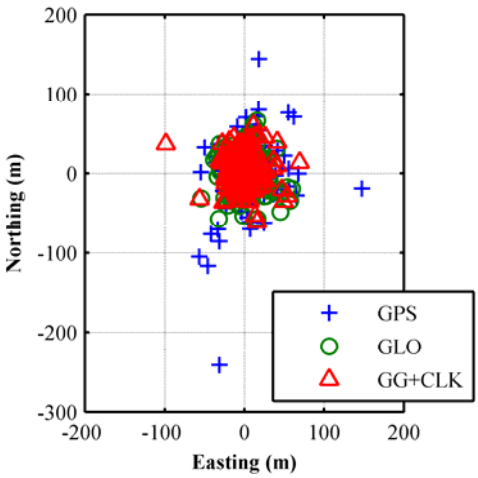

Figure 23: Scatter plot of horizontal position errors computed for the NavLab test, using all measurements with C/N_0 above 10 dB-Hz

In all cases the majority of the results are clustered within 100 m of the true position. The percentage of epochs for which a solution was computed is shown in Figure 24. It can be seen that there is a significant improvement in adding GLONASS, particularly as the receiver sensitivity decreases (i.e. the minimum C/N_0 threshold for the receiver increases). For example, for a receiver with a sensitivity of 16 dB-Hz, the availability of GPS solutions is approximately 70 %, while adding GLONASS brings this up to 85 %, and providing the system time offset yields 100 % solution availability in this case. Again the reader is reminded that these results are somewhat optimistic due to the interference rejection capabilities provided by the 1 s coherent integration time used in this test. Nonetheless the results are indicative of the benefits of adding GLONASS to the high sensitivity receiver.

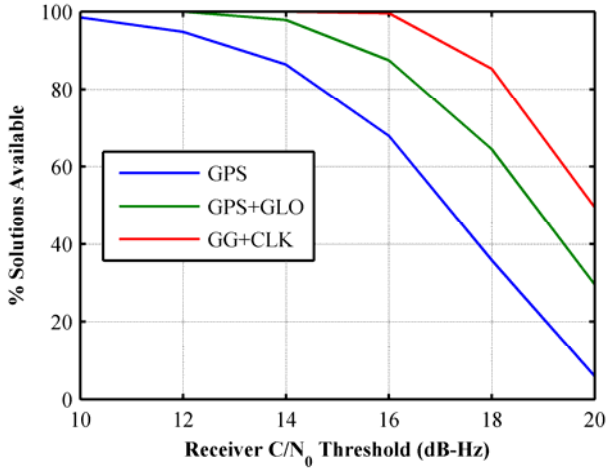

Figure 24: Percentage availability of position solutions vs receiver sensitivity for the NavLab test

Figure 25 provides an illustration of the impact of GLONASS on the geometry of the solution. Here the mean, maximum and minimum PDOP values obtained for valid solutions are presented. As with the WH scenario, the addition of GLONASS yields some improvement in the average PDOP values observed. In this case, however, the maximum values observed are significantly greater than those observed in the WH case. It is worth noting that position solutions obtained with a GDOP value greater than 20 are treated as invalid solutions by the navigation processor, hence the limited "maximum" PDOP values observed.

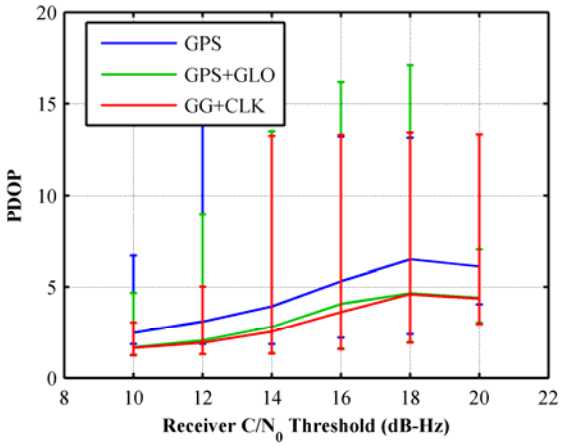

Figure 25: Mean, max and min PDOP values vs receiver sensitivity for the NavLab test. The continuous lines represent the mean value, the error bars report the maximum and minimum

Finally, the RMS position errors are plotted in Figure 26 and Figure 27. Here there is significant improvement in the horizontal position error, particular when the system time offset is provided in addition to the GLONASS measurements.

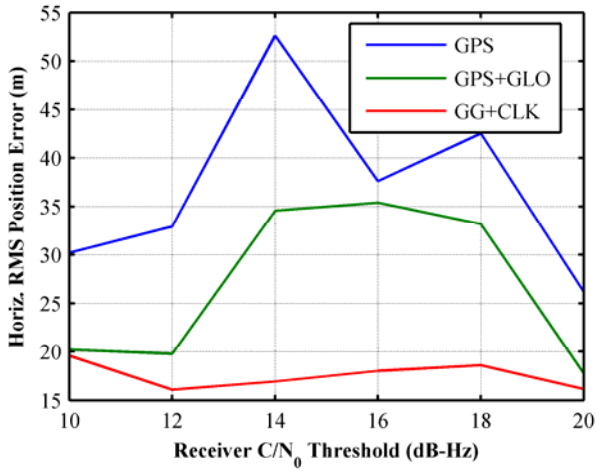

Figure 26: Horizontal RMS position error vs receiver sensitivity for the NavLab test

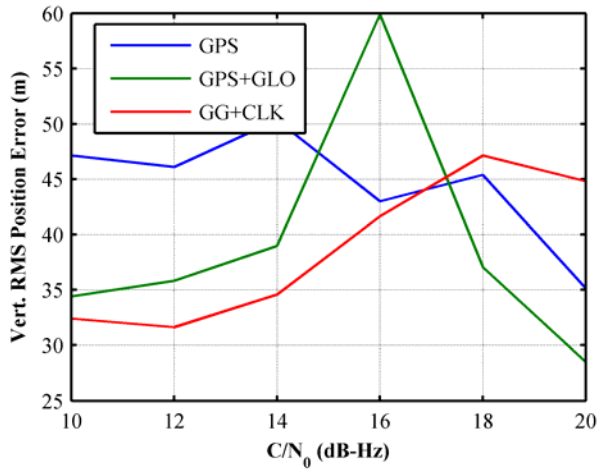

Figure 27: Vertical RMS position error vs receiver sensitivity for the NavLab test

The results of the vertical position are somewhat more mixed, particular for higher C/N_0 thresholds. For the 10 dB-Hz threshold there is, again, significant improvement (about 30 %) with the addition of GLONASS.

A NOTE ON INTEGRATION TIME

While the above analysis was based on an integration time of 1 s, this is not always practical. The receiver C/N_0 threshold can be approximated using a simple rule of thumb which states that the SNR at the correlator outputs should be greater than 10 dB for reliable detection. The C/N_0 and SNR are related by the simple equation:

$$SNR = 2C/N_0 T \quad \textbf{(3)}$$

A plot of required integration time vs C/N_0 is shown in Figure 28.

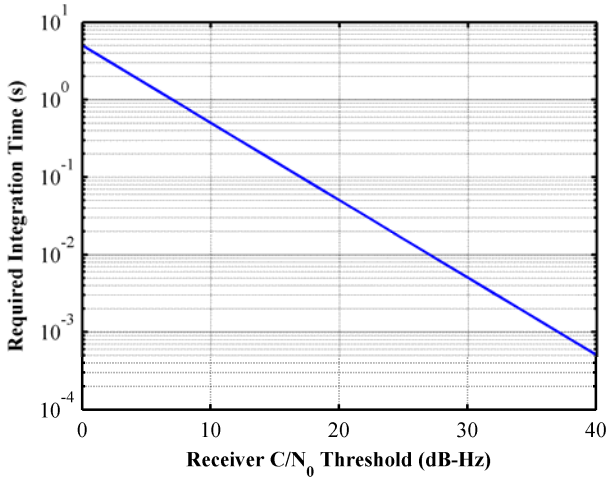

Figure 28: Required integration time vs receiver C/N_0 threshold

For example, for a receiver sensitivity of 10 dB-Hz, an integration time of 0.5 s is required. For a 100 ms integration time, the receiver sensitivity is approximately 17 dB-Hz. Of course, as discussed above, the impact of RF interference and signal cross correlation effects becomes greater as the integration time is decreased. So the results presented above for a given receiver sensitivity will be somewhat optimistic.

CONCLUSIONS

Using a reference/rover configuration to observe GNSS signals indoors, it has been shown that the behavior of the GPS and GLONASS L1 C/A signals are broadly similar in these environments. For the two test scenarios considered it appears that the availability and accuracy benefits of adding GLONASS become more significant the more challenging the environment. For moderate multipath or open sky environments, the HS-GPS receiver performs sufficiently well for many applications. For harsher environments (C/N_0 of the order of 10 dB-Hz), improvements in accuracy and availability of the order of 30 % were observed when GLONASS capability was added. The availability of an estimate of the GPS/GLONASS system time offset can make a significant difference in the availability and accuracy of solutions in scenarios with limited numbers of satellites.

While this work focused on the quality of pseudorange measurements obtained in a static mode in an indoor environment, future work will investigate the impact of dynamics, the quality of the Doppler measurements in urban environments, and reliability.

ACKNOWLEDGMENTS

The assistance of Shashank Satyanarayana and Pratibha Anantharamu for the data collection is greatly appreciated. The authors also wish to thank Nima Sadrieh for his idea and discussion on the inter-chassis synchronization technique.

This work was conducted with funding provided by iCORE, part of Alberta Innovates – Technology Future.

REFERENCES

GLONASS-ICD (2002). GLONASS Interface Control Document. Version 5, 2002, available from http://www.glonass-center.ru/ICD02_e.pdf.

Haddrell, T. and Pratt, A.R. (2001), "Understanding the Indoor GPS Signal", Proceedings of ION GPS-2001, Salt Lake City, UT, Sep 11-14.

Kaplan, Elliott (2006), "Understanding GPS Principle and Applications 2nd Edition," ARTECH house.

Lachapelle, G., S. Ryan, M.G. Petovello and J. Stephen (1997), "Augmentation of GPS/GLONASS for Vehicular Navigation under Signal Masking," Proceedings of the ION GPS-97, Kansas City, MO, September 16–19, pp. 1511–1519.

Lachapelle, G. (2009) Advanced GNSS Theory, ENGO 625 Lecture Notes, Department of Geomatics Engineering, University of Calgary.

Mitelman, A, P-L. Normark, M. Reidevall, J. Thor, O. Grönqvist and L. Magnusson (2006), "The Nordnav Indoor GNSS Reference Receiver", Proceedings of ION-GNSS 2006, Fort Worth, TX, September 26-29.

O'Driscoll, C., D. Borio, M.G. Petovello, T. Williams and G. Lachapelle (2009) The Soft Approach: A Recipe for a Multi-System, Multi-Frequency GNSS Receiver, Inside GNSS Magazine, Volume 4, Number 5, pp. 46-51

Satyanarayana, S, D. Borio and G. Lachapelle (2009), "GPS L1 Indoor Fading Characterization using Block Processing Techniques," ION GNSS 2009, Session D1, Savannah, GA, 22-25 September.

Watson, R., G. Lachapelle, R. Klukas, S. Turunen, S. Pietila, S. and I. Halivaara, (2005), "Investigating GPS Signals Indoors with Extreme High-Sensitivity Detection Techniques", *Navigation* **52**(4), pp. 199-213.